Global and Planetary Change 177 (2019) 56–68

Contents lists available at ScienceDirect

Global and Planetary Change

journal homepage: www.elsevier.com/locate/gloplacha

Deep-water formation variability in the north-western Mediterranean Sea during the last 2500 yr: A proxy validation with present-day data

Mercè Cisneros*, Isabel Cacho, Jaime Frigola, Anna Sanchez-Vidal, Antoni Calafat, Rut Pedrosa-Pàmies[1], Aitor Rumín-Caparrós, Miquel Canals

GRC Geociències Marines, Departament de Dinàmica de la Terra i de l'Oceà, Facultat de Ciències de la Terra, Universitat de Barcelona, Barcelona, Spain

ARTICLE INFO

Keywords:
Deep-water formation
Open-sea deep convection
Dense shelf water cascading
Western Mediterranean Deep Water
Last 2500 years
Mediterranean Sea

ABSTRACT

Here we investigate the sensitivity of deep-water formation in the north-western Mediterranean Sea to climate variability during the last 2500 yr. With this purpose, the grain-size parameter UP10 (fraction > 10 μm) is used as a proxy for intensity of deep-water circulation. Such a proxy is first validated through the analysis of oceanographic data collected from October 2012 to October 2014 by means of two deep-water mooring lines equipped with sediment traps and currentmeters in the Gulf of Lion and north of Minorca Island. Enhancements of deep current speed resulted from dense shelf water cascading and open-sea deep convection in February 2013 leading to dense-water formation. The grain-size distribution of settling particles from sediment traps collected during 2012–2013 shows a distinctive particle mode and high UP10 values correlated to deep-water formation. These data are consistent with grain-size values in sediment cores from the north of Minorca, thus supporting the validity of the UP10 parameter to reconstruct changes of intensity in deep-water formation and associated near-bottom currents.

The deep-water sediment record of the north of Minorca for the last 2.5 kyr shows that the strongest deep-water formation events occurred during relatively warm intervals, such as the Roman Period (123 BCE-470 CE[2]), the end of the Medieval Climate Anomaly (900–1275 CE) and the first part of the Little Ice Age (1275–1850 CE). By contrast, our data indicate a progressive reduction in the overturning conditions during the Early Middle Ages (470–900 CE) resulting in weaker deep-water formation events during most of the Medieval Climate Anomaly. Intense deep-water formation events appear to be mostly associated with periods of enhanced Evaporation-Precipitation balance rather than to buoyancy loss due to winter cooling only. Our results suggest that warm sea surface temperature during spring months could have played an important role by increasing the Evaporation–Precipitation balance and favouring buoyany loss by increased of salinity.

The comparison our data with other oceanographic and climatic records indicates a change in the proxy relation before and after the Early Middle Ages. Western Mediterranean Deep Water and Levantine Intermediate Water behave in opposite way after the Early Middle Ages, thus indicating that the previously proposed Mediterranean see-saw pattern in the Evaporation-Precipitation balance also influenced convection patterns in the basins during the last 1500 yr. These changes are discussed in the frame of different configurations of the North Atlantic Oscillation and East Atlantic/ West Russian modes of atmospheric variation.

1. Introduction

The western Mediterranean Sea, particularly the Gulf of Lion (GoL), is one of the few marine regions where deep-water formation (DWF) takes place and it occurs almost each winter through two oceanographic processes: dense shelf water cascading and open-sea deep convection (MEDOC Group, 1970; Canals et al., 2006; Durrieu de Madron et al., 2013; among others). These two processes are driven by intense sea-atmosphere heat exchanges, and the subsequent buoyancy loss of offshore waters, induced by cold, dry, and persistent N–NW winds, resulting in the formation of the Western Mediterranean Deep Water (WMDW) (Fig. 1).

The WMDW mass is an important component of the Mediterranean thermohaline circulation. It fills the deep basin locating in depths below

* Corresponding author.
E-mail address: mcisneros@ub.edu (M. Cisneros).
[1] Current address: The Ecosystems Center, Marine Biological Laboratory, Woods Hole, USA.
[2] BCE: Before Common Era years. CE: Common Era years.

https://doi.org/10.1016/j.gloplacha.2019.03.012
Received 2 August 2018; Received in revised form 20 March 2019; Accepted 20 March 2019
Available online 21 March 2019

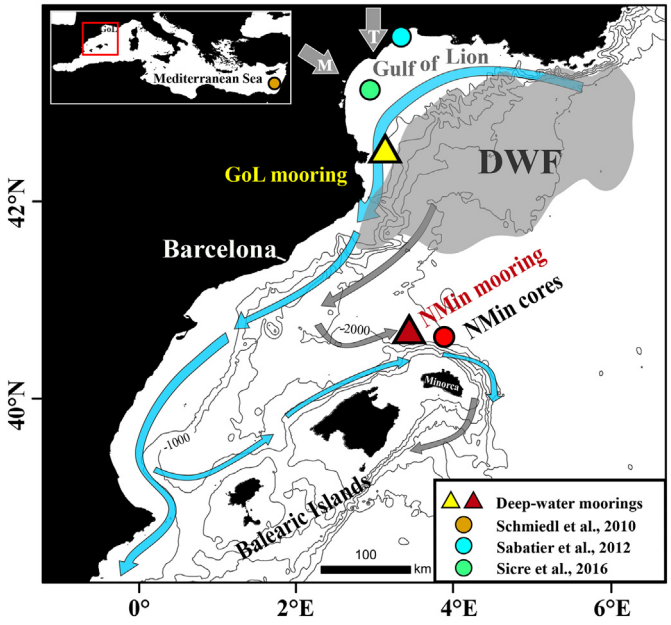

Fig. 1. Central-western Mediterranean Sea. Circles locate sediment cores. Red circle: NMin cores (this study); Green circle: KSGC-31 and GolHo-1B cores; blue circle: PB06 core; orange circle: SL 112 core in the Eastern Mediterranean. Triangles indicate NMin mooring (red, this study) and GoL mooring (yellow, Sanchez-Vidal et al., 2015). Grey short arrows: Tramuntana and Mistral winds. Blue and grey arrows: surface and deep sea circulation, respectively; the shadow area in the Gulf of Lion (GoL) indicates where the deep-water formation (DWF) occurs. (For interpretation of the references to colour in this figure legend, the reader is referred to the web version of this article.)

the Levantine Intermediate Water (LIW), and partly contributes in determining the characteristics of the Mediterranean outflow water (MOW) (Stommel et al., 1973; Lionello et al., 2006). Finally, changes in MOW could influence the Atlantic thermohaline circulation by enhancing the general salinity of the north Atlantic region (Bryden and Stommel, 1984; Lionello et al., 2006). In addition, the Mediterranean acts as a heat loss region from the Atlantic, since outcoming waters are colder than the incoming surface waters through the Strait of Gibraltar (Wu et al., 2007). Besides, changes in the strength of the Mediterranean thermohaline circulation associated with climate changes would also impact Mediterranean Sea Surface Temperature (SST) with immediate consequences in climate conditions of the adjacent areas (Somot et al., 2006). Changes in the SST would also have an impact on dense water formation rates and thus on hydrographic properties (Beuvier et al., 2010). Consequently, changes in DWF in the GoL could have oceanographic and climatic consequences at regional but also at large scales.

During the last years an intense effort has been carried out to increase the understanding on DWF in the western Mediterranean Sea and complete the existing instrumental data series (e.g.: Houpert et al., 2016; Somot et al., 2016; Estournel et al., 2016; Bosse et al., 2016, 2017; Durrieu de Madron et al., 2017). Long, high-quality and homogenised instrumental time-series covering the past few centuries exist for climate parameters like air temperature, precipitation and sea level pressure (Lionello et al., 2006 and references therein). Nevertheless, instrumental data on deep-water environments is still relatively short. In this way, paleorecords suppose a valuable contribution to enhance our temporal view of DWF evolution and better understand its connection with climate variability.

Some previous paleoceanographical studies have reconstructed changes in western Mediterranean DWF, particularly in relation to the last glacial millennial scale climate variability, when the GoL DWF weakened in relation to Dansgaard-Oeschger warm insterstadials (Cacho et al., 2000, 2006; Sierro et al., 2005; Frigola et al., 2008; Rodrigo-Gámiz et al., 2011). Or even, it has also been proposed that dense shelf water cascading may have played an important role during the Messinian salinity crisis (Roveri et al., 2014). Few evidences indicate some centennial scale Holocene oscillations in the intensity of deep-water currents associated with WMDW formation (Frigola et al., 2007) but these records lack the resolution for a detailed characterization of the historical record, especially the last two millennia. Past changes in deep convection in the eastern Mediterranean Sea have been intensively studied in relation to Sapropel deposition, particularly for the Holocene Sapropel 1 (Rohling et al., 2015 and references therein), but very little information exists for the last two millennia (Schmiedl et al., 2010; Incarbona et al., 2016).

The overall goal of this study is: i) to validate the application of the UP10 parameter in the Minorca promontory as a proxy of DWF in the GoL in base to oceanographical data, and then ii) to characterize the DWF evolution in the GoL during the last 2.5 kyr, to better understand its long-term variability and its relation with regional climate conditions. With this aim the generated records allow us to analyse the high frequency variability for climate/historical moments of the two millennium of the Common Era. The different climatic periods have been defined as follows (BCE = years before Common Era and, CE = Common Era): Talaiotic Period (TP, until 123 BCE), Roman Period (RP; 123 BCE-470 CE), "Early Middle Ages" (EMA; 470–900 CE), Medieval Climate Anomaly (MCA; 900–1275 CE), Little Ice Age (LIA; 1275–1850 CE) and, the Industrial Era (IE) as the most recent period (see Cisneros et al., 2016 for further information; EMA is equivalent to Dark Middle Ages).

The UP10 parameter has been analysed in two deep-sea multicores recovered north of Minorca Island (NMin) (Fig. 1). UP10 records with a preliminary age model were already published in Moreno et al. (2012). These age models were complemented and improved following a multiproxy chronology by Cisneros et al. (2016), where a 2 kyr SST stack record from a larger group of multicores was discussed.

2. Study area

2.1. Oceanographic settings

The Mediterranean Sea has been described as a 'miniature ocean' (Stanley, 1972; Margalef, 1985) that operates as a concentration basin (Bethoux et al., 1999), where the freshwater input does not compensate the overall evaporation. Consequently, Mediterranean dense waters are formed in specific basins filling intermediate and deep depths. Levantine Intermediate Water (LIW) forms in the eastern Mediterranean while Western Intermediate Water and Tyrrhenian Dense Water (MEDOC, 1970; Millot, 1999) form in the Western Mediterranean Basin at intermediate depths. DWF processes also take place in both basins forming the Eastern and Western Mediterranean Deep Water Masses (EMDW and WMDW, respectively).

The two main factors that seem to explain > 70% of the interannual variance of the DWF phenomenon are: i) the interannual variability of the winter-integrated buoyancy loss driven by the heat loss; and ii) the water column preconditioning before the convection mostly driven by both the heat and salt contents of the surface layer (Somot et al., 2016). Water mass properties in the western basin can be also related to variations in the characteristics of the surface and intermediate waters like Atlantic waters and LIW (Schroeder et al., 2011; Somot et al., 2016; Estournel et al., 2016).

The exchange of energy between the atmosphere and the sea surface takes place through net air-sea heat exchange, which is the sum of four fluxes: latent and sensible heat fluxes (linearly proportional to the wind speed and the air-sea temperature or humidity difference) and, short and long-wave radiation fluxes (function of air temperature, humidity, and cloudiness) (Deser et al., 2010).

In addition, dense waters in the GoL can be also originated by dense shelf water cascading process (Canals et al., 2006), flowing down the

Table 1
Sediment trap samples from the GoL (Cap de Creus Canyon; CCC1000) and NMin (MIN-I) calculated in this study to validate UP10. "t" corresponds to the total grain-size fraction and "dc" to de-carbonated. TMF: Total Mass Flux. UP10 proxy integrates the grain-size fraction coarser than 10 μm.

Sample	Opening day	Closing day	TMF (mg m^{-2} d^{-1})	UP10	Near-bottom current velocity peaks (cm s^{-1})	Hydrological situation
CCC1000-III-3 (t)	16/1/12	1/2/12	3639.4	27.5	11	Pre-cascading
CCC1000-III-4 (t)	1/2/12	16/2/12	68,156.9	51.2	126	Cascading (start)
CCC1000-V4 (dc)	1/2/13	15/2/13	3102.0	21.5	13	Pre-cascading
CCC1000-V5 (dc)	15/2/13	1/3/13	64,130.1	42.2	84	Cascading
CCC1000-V6 (dc)	1/3/13	16/3/13	25,674.1	29.3	82	Post-cascading
MIN-I-6 (t)	1/3/13	1/4/13	479.4	31.4	24	Pre-open sea deep convection (and start)
MIN-I-6 (dc)	1/3/13	1/4/13		33.7		
MIN-I-8 (t)	1/4/13	1/6/13	896.3	42.4	23	Open sea deep convection (and post)
MIN-I-8 (dc)	1/4/13	1/6/13		38.2		

slope towards the deep basin, interacting with the open-sea convected waters (Bethoux et al., 2002; Durrieu de Madron et al., 2013, 2017). These cascading events are also linked to cold, dry, and persistent N–NW winds that induce sea-atmosphere heat losses. Although major open-sea convection events can occur while cascading is weak (Durrieu de Madron et al., 2017) and, the WMDW mass is mainly renovated by the open-sea convection process, the cascading contribution has also been proposed as a relevant contributor (Bethoux et al., 2002; Puig et al., 2013; Durrieu de Madron et al., 2013).

2.2. Controls on Mediterranean inter-annual climate variability

The Mediterranean climate is influenced by both mid-latitude and tropical dynamics (Lionello et al., 2006), constituting a transitional zone, high sensitive to climate variations. The seasonal variability is characterized by mild wet winters and warm to hot, dry summers. Processes of annual formation of WMDW are very much related to specific local atmospheric configuration (López-Jurado et al., 2005). Direct observations during recent years describe four main winter modes of interannual atmospheric variability in the North Atlantic/Europe region that exert a control on air-sea heat exchange in the Mediterranean Sea: i) the North Atlantic Oscillation (NAO); ii) the East Atlantic (EA); iii) the Scandinavian (SCAN); and iv) the East Atlantic/West Russian (EA/WR) patterns (Cassou et al., 2010; Josey et al., 2011). i) The NAO can be defined as a large-scale meridional see-saw on atmospheric pressures along the North Atlantic sector (Hurrell, 1995). The remaining modes of atmospheric variability present a less clear picture due to have signature only during part of the year, among another factors (Trigo et al., 2006). ii) The EA pattern, first described by Wallace and Gutzler (1981), consists of a north-south pressure dipole structurally similar to NAO but with the centres spanning from east to west in the North Atlantic and showing a stronger subtropical connection in the lower-latitude center (Barnston and Livezey, 1987). iii) The SCAN pattern has a southwest-northeast pressure dipole with the stronger pole centred to the east of Scandinavia. It influences the generation of northern European precipitation anomalies (Bueh and Nakamura, 2007) and in the Mediterranean region has been considered to have weaker influence than the other modes (Josey et al., 2011). Lastly, iv) the EA/WR pattern has been proposed to impact the Mediterranean region rainfall (Krichak and Alpert, 2005) and its heat loss in winter, creating an east-west dipole structure over the Mediterranean stronger than that from the NAO.

Different combinations between the atmospheric patterns can cause distinct effects on the present-day climate. For instance, NAO/EA configurations with the same (opposite) sign have been coincident with homogeneous (heterogeneous) spatial correlations of both precipitation and temperature (Comas-Bru and McDermott, 2014). In particular, during years with numerous days of predominant EA patterns and only a few number of NAO- days, correspond to years of intense DWF in the north-western Mediterranean (NWMed) region (Bethoux et al., 2002; Puig et al., 2013; Durrieu de Madron et al., 2013).

3. Material and methods

3.1. Mooring measurements and sediment cores

Present and past deep-sea conditions have been evaluated combining data from two mooring lines and two sediment cores from the same area (Fig. 1).

The first mooring (CCC1000) was deployed in the GoL margin in the axis of the Cap de Creus Canyon at 968 m of water depth (henceforth GoL-mooring; 42°18.88′N, 3°33.52′E) during October 2012–May 2014. The mooring was equipped with a Nortek Aquadopp currentmeter placed at 23 m above the bottom (mab). Sampling intervals were set at 20 min during the period 2012–13 and at 15 min during 2013–2014, respectively. This mooring also included a Technicap PPS 4/3 cylindro-conical sediment trap at 25 mab, with a sampling period of 15 days (Table 1). More details about this mooring are described in Sanchez-Vidal et al. (2015).

The second mooring (MIN-I) was deployed in the sediment drift built by the action of the southward branch of the WMDW north of Minorca at 2052 m of water depth (henceforth NMin-mooring; 40°28.05′N, 03°40.64′E) during October 2012–October 2014. The mooring was equipped with a Nortek Aquadopp currentmeter placed at 5 mab and with a SBE37 at 5 mab (2012 − 2013) or 25 mab (2013–2014). Sampling intervals were set at 15 min (SBE37 and Aquadopp) in 2012–2013, and 10 min (SBE37) and 30 min (Aquadopp) in 2013–2014. It was also equipped with a Technicap PPS 3/3 cylindro-conical sediment trap at 25 mab, with a sampling period ranging from one or two months (Table 1).

MINMC06–1 and MINMC06–2 multicores (henceforth NMin1 and NMin2; 40°29′ N, 04°01′ E; 2391 m water depth; 31 cm and 32.5 cm core length, respectively) were recovered in the north Minorca sediment drift in the path of the southward branch of the S-SE flowing WMDW, very close to the NMin-mooring location (Fig. 1). The suitability of this location for detailed paleoceanographic reconstructions was already pointed out by previous studies (Sierro et al., 2005; Frigola et al., 2007, 2008; Cisneros et al., 2016). More detailed information on the sediment drift formation and characteristics can be found in Velasco et al. (1996) and Frigola et al. (2007).

3.2. Particle size-characterization

The grain-size distribution of the total and de-carbonated fractions was analysed in both NMIN cores (0.5 cm resolution) and in the settling particles collected with the sediment traps of the two moorings. The analysed settling particles corresponds to periods comprised into 2012–2013 (see Table 1) and represent conditions of before, during and after a DWF event.

Grain size analyses were performed using a Coulter LS230 Laser Diffraction Particle Size Analyser (CLS). Prior to analysis, on the one hand, organic matter from dried samples was removed with a 10% H_2O_2 solution, thus allowing to obtain the total fraction grain size

distribution. On the other hand, the lithic grain-size particle distribution was obtained after 1 M HCl treatments of samples for carbonates removal, thus obtaining the de-carbonated fraction. In core NMin2 both total and de-carbonated fractions were analysed while in NMin1, the longest core, only the total fraction was analysed. For settling particle samples a combination of both total and de-carbonated fraction was analysed (Table 1). The total fraction of the sediment integrates the lithic fraction, including detrital carbonates, but also carbonate tests representing local biological production. By these reason, the de-carbonated fraction is considered to better represent the bottom currents intensity, since the local pelagic productivity signal has been removed with the carbonates (McCave et al., 1995). However, carbonates removal also affects those from detrital origin, mostly fines, and consequently the grain-size percentages of the de-carbonated fraction use to show higher values, due to the closure effect to 100%. In addition, differences between total and de-carbonate fractions from the same core can also be affected by down-core differences in carbonate content. Thus, the down-core discussion and interpretations are centred in the results obtained with the de-carbonated fraction from core NMin2. However, total fraction results from NMin1 are also incorporated in the discussion since it allows the extension of the record to the RP. This is supported by the relatively good correlation between total and de-carbonate fractions from core NMin2 (Fig. S1).

CLS measures sizes between 0.04 μm and 2000 μm determining grain-size distributions as volume percentages based on diffraction laws (McCave et al., 1986; Agrawal et al., 1991). It is assumed that this diffraction is given by spherical particles and the particle size is provided as an "equivalent spherical diameter". For this reason, laser diffraction methods are claimed to underestimate plate-shaped clay mineral percentages. To correct this underestimation, content of clays included sizes until 8 μm, as proposed by Konert and Vandenberghe (1997). CLS accuracy and repeatability (precision) were tested by running the standard LS size control G15 and using glass beads with pre-defined parameters, which gave standard deviations of 2.4% and coefficients of variation better than 0.3%, respectively.

Particle size distributions are discussed considering the grain-size fraction coarser than 10 μm (UP10 fraction), which was previously applied as an indicator of deep currents variability in this area (Frigola et al., 2007). Other grain-size parameters different to the UP10 are often used in the literature for the study of deep-water currents intensity, as is the case of the sortable silt (SS) fraction (McCave et al., 1995, 2017) and the silt/clay ratio (Hall and McCave, 2000). The SS fraction (10–63 μm) is defined as the coarser fraction of the silt with noncohesive behaviour during transport and deposition (McCave et al., 1995). Thus, neither the SS nor the silt/clay parameters take into account the fine sand subpopulation (> 63 μm), which is integrated in the UP10 fraction that, as discussed below, could be reworked by strong contour currents (Frigola et al., 2007, 2008). Nevertheless, we have compared the results for the three mentioned grain-size parameters in both studied cores and settling particles measurements from NMin and the results are comparable (Fig. S1).

4. Results and discussion

4.1. Winter 2013: dense shelf water cascading and open-sea deep convection

Deep oceanographic conditions (temperature and current velocity) obtained by the moored instruments in the GoL and NMin (comprised into October 2012–October 2014), presented by first time in the present study, are shown in Fig. 2 together with meteorological data. The average deep-water temperature recorded during October 2012–May 2014 in both sites is very similar, around 13.2 °C (Fig. 2f–g). However, the GoL-mooring time serie shows important changes in winter 2013 in contrast to the rather stable temperatures from the NMin-mooring. These GoL temperature changes involved a drop of 1.63 °C (from 13.07 to 11.44 °C) by the end of February 2013 in the Cap de Creus canyon axis, while downcanyon near-bottom current speeds enhanced up to 84 cm s^{-1} (Fig. 2f–g). Both temperature drop and downcanyon flow evidences the occurrence of a dense shelf water cascading event. Cold and dry northerly winds produced cooling and densification of surface waters in the continental shelf (Fig. 2b–c) and, subsequently, waters sunk, overflowed the shelf edge, and cascaded downslope through south-west GoL's submarine canyons to at least 1000 m depth where the mooring was located. The winter 2013 cascading event has been described as a reemergence of the stronger one occurring in winter 2012 (1–3 °C drop and currents up to 125 cm s^{-1}) (Durrieu de Madron et al., 2013; Sanchez-Vidal et al., 2015). 'Reemergence' refers to the easy reproduction of a deep and cold mixed layer because of the thermal anomalies of the previous year (Somavilla et al., 2009).

The same intense atmospheric forcings in February 2013 also triggered open-sea convection offshore (Waldman et al., 2017; Durrieu de Madron et al., 2017; Houpert et al., 2016), after increase air–sea heat fluxes (Fig. S2). Sea surface cooling and destabilization of the water column involved deep vertical mixing and an exceptional bottom reaching convection event, as also shown as a very low chlorophyll patch in February 2013 (Fig. S3 left). After this intense convective episode, long-lived mesoscale eddies were formed and the new WMDW was advected southwestwards towards the north of Minorca (Testor and Gascard, 2006; Bosse et al., 2016, 2017; Waldman et al., 2017; Margirier et al., 2017). A series of peaks in near-bottom currents, up to 24 cm s^{-1} were detected in the NMin-mooring during February–April 2013 and one of them is coincident with the described event in the GoL-mooring (Fig. 2g). These NMin highest velocities are in agreement with those maxima (28 cm s^{-1}) recorded by the LION-mooring line located in the centre of open-ocean convection zone during the end of February 2013 (Durrieu de Madron et al., 2017). Therefore, spreading of bottom-reaching open-sea convection may have reached north Minorca as well.

Overall, the same atmospheric forcing triggered dense water formation in the continental shelf and open-sea convection, and both lead to increased near-bottom current speeds. In any case, both DWF processes have demonstrated to produce active resuspension and redistribution of deep sediments (Canals et al., 2006; Stabholz et al., 2013; Puig et al., 2013). Therefore, we hypothesise that sediment cores from the NMin sediment drift are sensitive to the described changes in deep currents associated with WMDW production processes and we propose their applicability to reconstruct the operation mode of this convection cell during the last 2.5 kyr.

4.2. UP10: proxy for DWF in the past

We have evaluated the effects of increased bottom currents during DWF events on present-day sediment transport and particle grain-size distributions in the GoL and NMin, and investigated their linkage to the grain-size of the sedimentary record for the study of DWF in the recent past.

On the one hand, grain-size distributions of settling particles in both investigated areas when no DWF occurred show 3 main modes at 0.3, 5–10 (dominant class) and 20–40 μm, and UP10 values ranging from 21.5–33.7% (Fig. 3a–b). In contrast, during DWF there is a shift in grain-size towards coarser values, characterized by the appearance of a mode > 40 (and ~ < 100 μm), which is hardly present in the other samples (Fig. 3a–b). Thus, maxima UP10 values occurred during the period of DWF (38.2–51.2%) together with maxima particle fluxes and the highest variability in the grain-size distribution (Fig. 3a; Table 1). In fact, transport of large amounts of suspended coarse sediments from the continental shelf down-canyon towards the deep basin was already previously described during GoL cascading currents (Canals et al., 2006; Puig et al., 2008; Sanchez-Vidal et al., 2008). Furthermore, the intensification of deep currents NMin due to DWF should be able to resuspend and transport coarse particles (Martín et al., 2010; Stabholz et al., 2013). Overall, this evidences that DWF, either through cascading

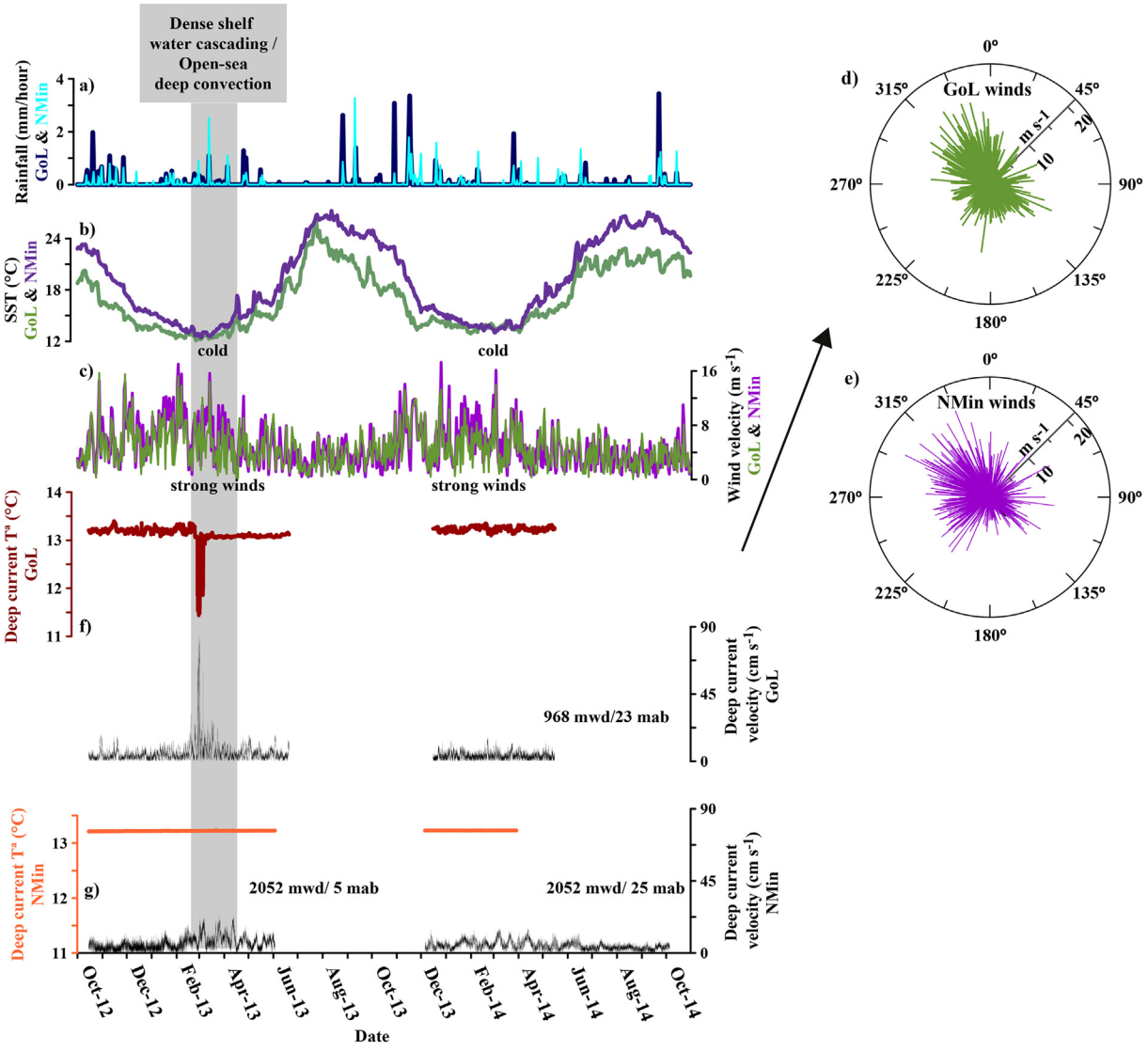

Fig. 2. Meteorological conditions and mooring measurements during October 2012–October 2014 in the Gulf of Lion (GoL) and north Minorca (NMin). Meteorological data: a) Precipitation in GoL (http://www.esrl.noaa.gov/psd/in) and Mallorca Island (www.balearsmeteo.com/sant_lorenzo); b–e) Sea Surface Temperature (SST), wind velocity and direction (http://www.esrl.noaa.gov/psd/in). Oceanographic data obtained from GoL and NMIN moorings (this study): f–g) Near-bottom current temperature and velocity in each mooring site. Depths of the moorings (mwd: m water depth) and of the currentmeters (mab: meters above the bottom) are also indicated. The grey vertical bar indicates the period of deep-water formation (dense shelf water cascading/open-deep sea convection).

or convection, has a direct impact on the grain-size distribution and the UP10 of settling particles in both regions.

On the other hand, grain-size distributions from sediment core samples recovered in the NMin sediment drift show similar modes to those described for settling particles. Thus, samples with the finest/coarsest grain-size distributions from NMin1 and NMin2 cores have a comparable grain-size distribution of setting particles when no DWF occurred/during DWF, respectively (Fig. 3c–f). The good resemblance in the grain-size distribution of settling particles and the sedimentary record supports the interpretation of high UP10 values from samples of the NMin sediment drift as a proxy of increased current velocities near the seafloor related to DWF (Fig. 4). Most of the analysed sediment core samples show very similar distributions to that of settling particles corresponding to relatively calmed conditions. However, some intervals from the sediment cores are characterized by the appearance of sediment mode populations well above 40 μm, between 100 and 120 μm and up ~220 μm, and in some specific intervals arrive up to ~300 and 400 μm. These very coarse samples also show high mode variability, minor sorting, and high UP10 values (Figs. 3 and 4). Such coarse grain populations were not detected in settling particle, possibly because sediment core samples may reflect deep current speeds from stronger DWF events than those from year 2013 but also it needs to be considered that sediment traps collect particles several meters above the bottom (25 mab) and may not have the same intensity than those at the actual sea floor. These coarser sediment mode populations could possibly correspond to lag deposits, like a consequence of armouring processes (Hüneke and Stow, 2008; Gambacort et al., 2014).

Maximum near bottom current speeds recorded during the spreading of dense water during winter 2013 (24 cm s^{-1}, at 25 mab) exceed the threshold to transport particles up to 40 μm, as calculated by the Sedtrans model (Li and Amos, 2001). However, some of the down-core sediment samples with modes up to 220 μm, would require currents up to 39 cm s^{-1} at the bottom and 61 cm s^{-1} at 25 mab to start their transport. This difference in the transport capacity of bottom currents and those at 25 mab may explain in part the general coarser modes found in the sediment cores. The coarsest grain-size distributions of these down-core samples are ~300 and 400 μm and would require bottom-currents up to 45 and 47 cm s^{-1} respectively, to start their

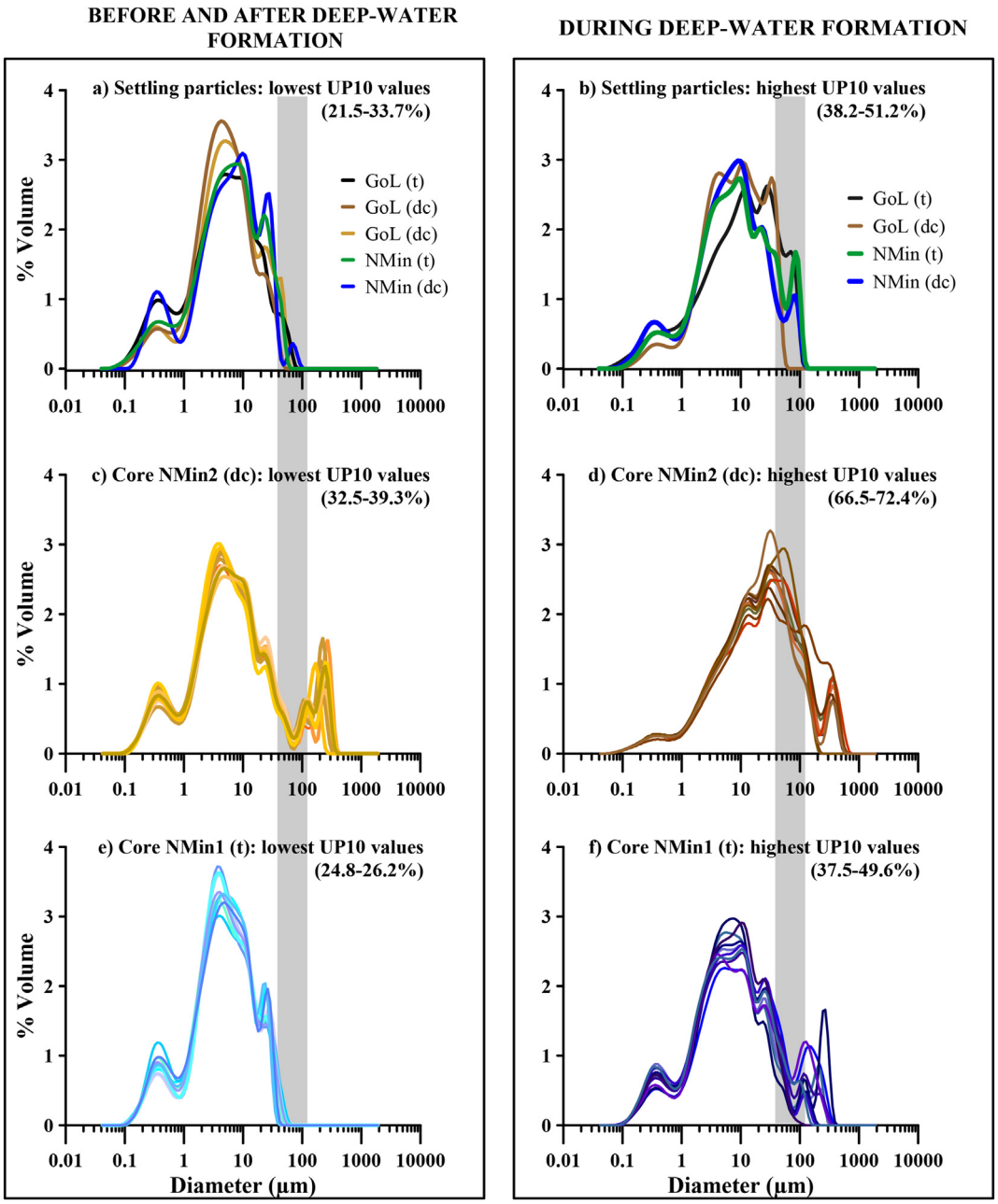

Fig. 3. Grain-size modal distributions from settling particles (a–b) and multicores (c–f). Figures of the left correspond to periods before and after the Deep-Water Formation (DWF) and those in the right to periods during DWF. (t) corresponds to total grain-size fraction and (dc) to de-carbonated. GoL samples correspond to Mooring CCC1000 and NMin samples to Mooring MIN-I (see Table 1 for entire code of samples). c–d) the 10 highest and 10 lowest UP10 values of NMin2 core (dc), respectively and; e–f) the 10 highest and 10 lowest UP10 values of NMin1 core (t). Vertical grey bars indicate grain-size particle band from ~40 to 100 µm.

transport at the sea bottom. Although these calculated bottom velocities were not recorded in 2013 by the NMin mooring, they are comparable to the maximum velocities detected in the centre of the basin (45 cm s^{-1} at 30 mab) during the 2013 DWF event (Durrieu de Madron et al., 2017). Overall, this suggests that during some periods of the past, DWF events could have been more energetic than that recorded in 2013, although most of the studied time period were of similar intensity or even weaker (Fig. 4).

Consequently, these results supports that currents in the studied region can be strong enough to transport fine sand particles and, in consequence, the UP10 fraction better represent transport changes in the whole particle size spectrum of the region and thus, this is a reliable proxy for deep-water intensity currents related to DWF events in the GoL (Frigola et al., 2007).

4.3. DWF variability: the last 2500 years

Long-term trends from the UP10 record of the de-carbonated fraction of NMin2 core and that of the total fraction of NMin1 core present a significant correlation for the common spanned period ($r = 0.3$, p value ≤ 0.0465) (Fig. 4). The major differences between both cores are observed during the EMA. UP10 percentages are always higher in the de-carbonated than in the total samples, likely due to removal of fine carbonate particles and the closure effect of 100% (c.f. Section 3.2). For this reason, differences in absolute values between the two cores (Fig. 3) mainly reflect different sample treatment and not different sensitivity to the speed changes. Note that UP10% are very comparable between the two records measured in the total fraction (Fig. S1). Consequently, oscillations in the UP10 record of the total fraction from

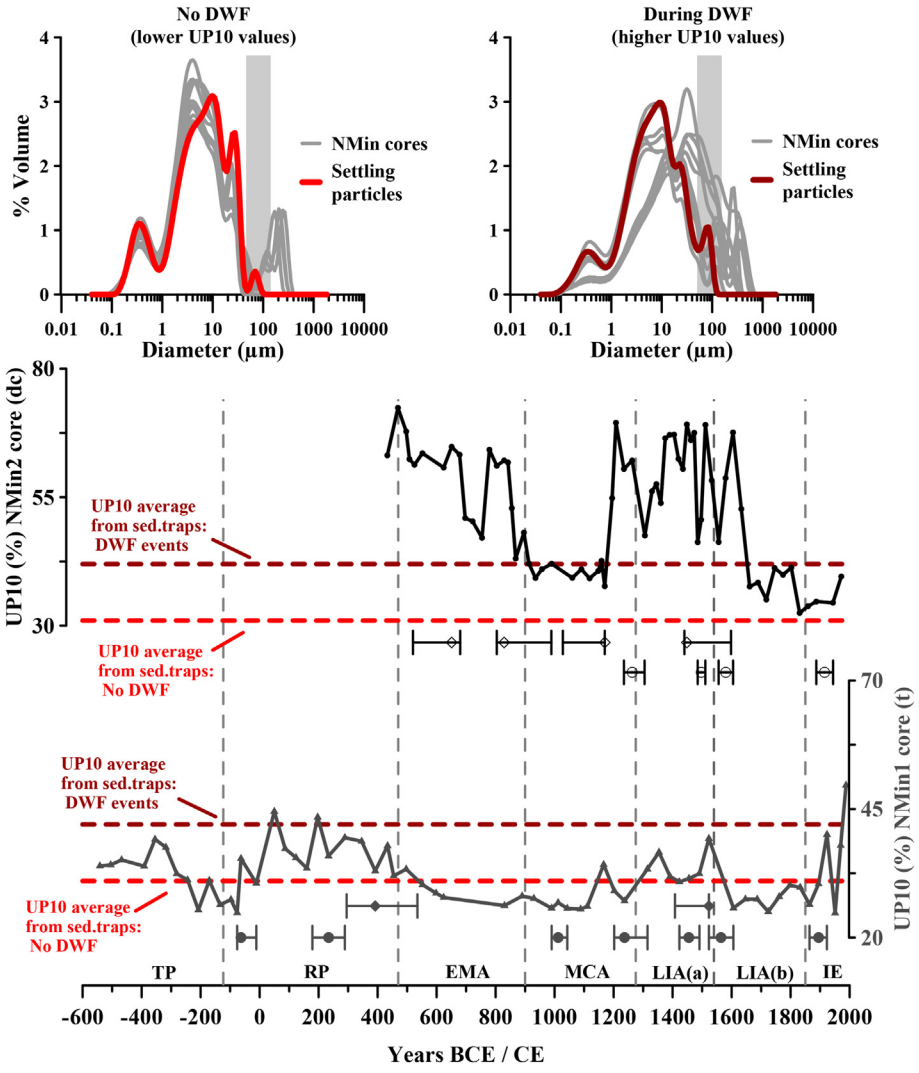

Fig. 4. Upper panels: grain-size distribution from NMin sediment cores (grey) and from the de-carbonated fraction from settling particles (red) in NMin during deep-water formation (DWF; right) and during periods without DWF (left). Data from MIN cores represent the 10 samples with highest (right) and the 10 lowest (left) UP10 values. Vertical grey bars indicate grain-size particle band from ~40 to 100 µm.

Lower panel: UP10 proxy records (total fraction > 10 µm) for NMin2 cores (black) and NMin1 (grey) during the last 2.5 kyr. (dc) corresponds to the de-carbonated grain-size fraction and (t) to the total grain-size fraction. Age control points with their associated error bars are shown below each core, diamonds represent absolute calibrated ^{14}C AMS dates and circles represent tie points using different chrono-stratigraphic markers (Cisneros et al., 2016 for details). Horizontal dashed lines represent average UP10 values obtained during DWF (dark red) and before or after DWF (light red) in settling particle from NMin. Years are expressed as Before Common Era (BCE; negative years) and Common Era (CE). Vertical dashed lines indicates the limits of the discussed periods: TP: Talaiotic Period; RP: Roman Period, 123 BCE-470 CE; EMA: Early Middle Ages, 470–900 CE; MCA: Medieval Climate Anomaly, 900–1275 CE; LIA: Little Ice Age, 1275–1850 CE; IE: Industrial Era. (For interpretation of the references to colour in this figure legend, the reader is referred to the web version of this article.)

NMin1 core can be mainly derived from deep current intensity changes, thus allowing expanding the studied period to 500 BCE. Thus, both de-carbonate and total UP10 records from NMin2 and NMin1 cores, respectively, will be discussed in parallel.

Two main intervals with high values of the UP10 fraction suggest intense DWF in the GoL during the last 2.5 kyr. The first time interval includes the RP and the EMA (~0–900 CE), while the second one corresponds to the end of the MCA and the LIAa (~1150–1600 CE). Relative low values of the UP10 fraction during the MCA, and especially those during the end of the LIAb and the beginning of the IE, suggest reduced DWF conditions. During RP and EMA remarkable winter vertical mixing has been already suggested by Margaritelli et al. (2018) through observations of foraminiferal assemblages studied in cores recovered in NMin.

4.3.1. The role of SST and humidity conditions

Considering that cold and dry northerly winds promote DWF events in the GoL, it could be expected that cold winters were coincident with intense DWF. This relation can be reviewed for the past using our GoL-DWF record and an alkenone-SST record from the GoL (Sicre et al., 2016) (Fig. 5a). The alkenone-SST record is interpreted to mostly reflect annual average temperatures, although slightly biased towards the cold season since no alkenone production occurs during summer months in the Mediterranean (Cacho et al., 1999; Sicre et al., 2016; Cisneros et al., 2016). Relatively cold SST in the GoL are coincident with high UP10 ($r = -0.3$, p value ≤ 0.0270) during the last 1.5 kyr (Fig. 5a). However, focusing on the multi-centennial trends, not significant correlations have been observed during each of the spanned periods except for the RP ($r = 0.5$, p value ≤ 0.0175).

A further insight in the past connection between GoL-DWF and SST conditions can be performed through the study of two additional SST-stack records alkenone and Mg/Ca proxies derived, respectively, which were produced in a multi-core collection from the NMin region, including those cores used in our UP10 records (Cisneros et al., 2016). Correlation of the NMin alkenone-SST and Mg/Ca-SST records with the DWF record ($r = 0.4$, p value ≤ 0.0002 and $r = 0.6$, p value = 0, respectively) suggests that strongest DWF events occurred preferentially during periods with relatively warm SST (Fig. 5a and b). According to that, the strongest DWF events preferably occurred during relatively warm periods such as the RP ($r = 0.7$, p value = 0), or the end of the MCA and LIAa. The Mg/Ca-SST drop during the EMA is also accompanied by a relative reduction in the intensity of the DWF events ($r = 0.8$, p value = 0). In this case, the record comparison does not have any time uncertainty since both records share the same chronology (Cisneros et al., 2016). This relation is surprising since Mg/Ca-SST record from the planktonic foraminifera *Globigerina bulloides* has been interpreted in this region to reflect mostly spring season conditions (Cisneros et al., 2016) and it is not reflecting any cooling intensification associated with the strong DWF periods. Therefore, this proxy comparison suggests that SST was not the main factor controlling past changes in GoL-DWF.

Changes in the hydrological cycle can also be critical determining

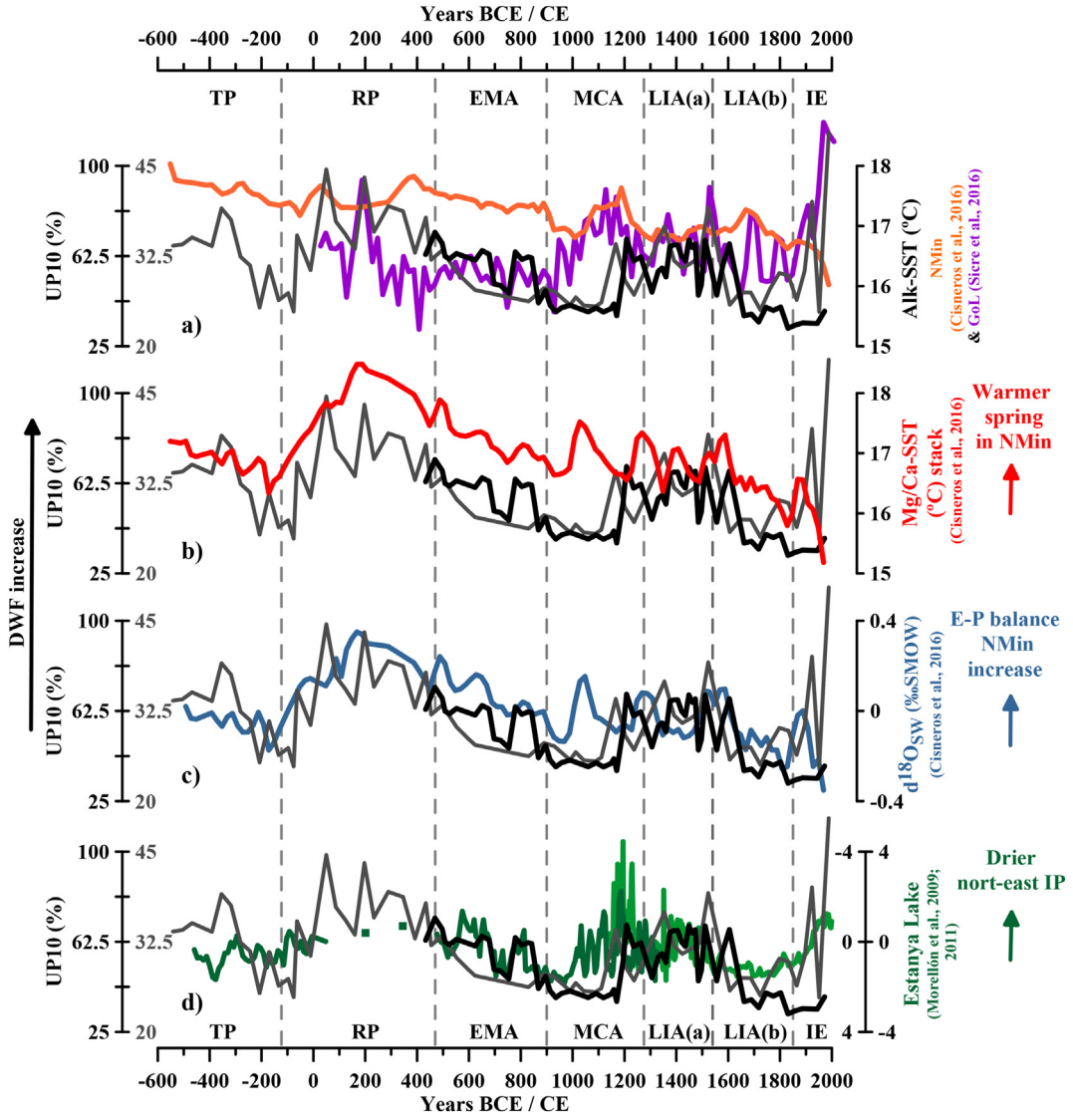

Fig. 5. UP10 record from NMin2 core (de-carbonated grain-size fraction) and from NMin1 core (total grain-size fraction) are represented in black and grey, respectively, using left axes and compared to: a) Alk-SST from Gulf of Lion (GoL) plotted at 20 yr-time steps (Sicre et al., 2016) and, Alk-SST from NMin (Cisneros et al., 2016); b) Mg/Ca-SST from NMin (Cisneros et al., 2016); c) Evaporation-Precipitation (E-P) balance reconstructed by $\delta^{18}O_{sw}$ in NMin cores (Cisneros et al., 2016); d) Salinity reconstruction in the north-east Iberian Peninsula (IP) from Estanya Lake salinity (PCA 2) (Morellón et al., 2009; Morellón et al., 2011).

surface salinity and thus the intensity of DWF. In order to explore this, we have compared the $\delta^{18}O_{sw}$ stack record, based on the Mg/Ca-SST stack reconstruction discussed above (Fig. 5b) (Cisneros et al., 2016), with our UP10 record (Fig. 5c). The $\delta^{18}O_{sw}$ record is interpreted to reflect Evaporation-Precipitation (E-P) balance, which in this case would potentially integrate a wide region from the Western Mediterranean Basin. At multi-centennial time-scale and for the last 1.5 kyr, they show a good correlation ($r = 0.6$, p value = 0) indicating intensification (weakening) of DWF in the GoL generally during increased (decreased) E-P sea-water balances. This positive relation is particularly clear for the EMA ($r = 0.7$, p value ≤ 0.0001) and the LIAb ($r = 0.8$, p value ≤ 0.0008) as well as for the RP (r = 0.6, p value ≤ 0.0011). An additional humidity/aridity record, in this case more sensitive to local precipitation, is the salinity reconstruction from Estanya Lake, north-eastern Iberian Peninsula (Morellón et al., 2009, 2011). Despite time uncertainties between the records (Fig. 5d), they show a coherent pattern of stoked DWF (high UP10 values) during drier conditions (saltier waters) in Estanya Lake ($r = 0.4$, p value ≤ 0.0004). This is the case for the second half of the MCA and LIA(a) while the more humid conditions of the LIA(b) are coincident with weaker DWF. The low resolution of the record for the RP does not allow analysing this time interval.

Overall, strong DWF (maximum UP10 values) occurred during both cold and relatively warm periods in the GoL. This could be partly explained by the fact that net heat flux during wintertime, which is mainly dominated by the latent heat flux (Houpert et al., 2016), is not directly reflected in the SST records. Latent heat flux, and to a lesser extent sensible heat, control anomalies in the winter net heat exchanges in the GoL (Josey, 2003; Schroeder et al., 2010). Regarding to the remarkable similarity between our DWF and the Mg/Ca-SST records (Fig. 5b), warm spring SST could be also related to drier conditions, thus both favouring E-P balance and a subsequent increase of salinity. For example, this can be observed at the end of the MCA, with a relative increase in SST coincident with drier conditions in the north-east Iberia, thus allowing an intensification of DWF. More research is needed in order to better understand the relationship between changes in SST and hydrology conditions on DWF in this region. However, similar results have been also observed in south-west Australia, a region that is also located in a Mediterranean climate zone (Pattiaratchi et al., 2011). Consequently, these results further support that SST have not been the

only critical factor determining the intensification of DWF during the last 2.5 kyr, and point that buoyancy loss, although might be ultimately triggered by SST cooling, is highly controlled or modulated by E-P balance and thus hydrological conditions in the north-western Mediterranean region. This is consistent with the discussed changes in regional humidity patterns which could contribute to the buoyancy-loss and preconditioning of the Mediterranean waters by enhancing E-P balance. This preconditioning has been considered the second driving factor in deep water convection (Somot et al., 2016), favouring the weakening of the vertical stratification due to reduced freshwater inputs and subsequent increases in surface salinities (Stommel, 1972). This preconditioning mechanism has been proposed to occur towards late-summer early-autumn, when storm winds and water cooling contribute to mix the surface layer and to progressively erode the seasonal thermocline (Puig et al., 2013). Further research in needed regarding past changes in surface salinity conditions in the paleoceanographic record in order to disentangle the relationship between surface conditions and deep-water convection.

4.3.2. Atmospheric teleconnections and links with the Eastern Mediterranean Basin

In order to assess potential connections between our reconstructed GoL-DWF record with changes in the wind system over the GoL during the last 1.5 kyr, we compare it with a storm activity record based on lagoon sediments from the GoL (Sabatier et al., 2012). Both records show certain similarity ($r = -0.3$, p value ≤ 0.0249) indicating that periods of enhanced storm activity were generally coincident with strong DWF activity (Fig. 6a). The higher coherence between high/low UP10 values and high/low GoL-storm activity is observed during EMA ($r = -0.8$, p value ≤ 0.001). Correlation is also remarkable during RP ($r = -0.5$, p value ≤ 0.0032), MCA (r = −0.5, p value ≤ 0.0191) and LIAa ($r = -0.6$, p value ≤ 0.0236) but lower or even opposite correlation occurs during the LIAb and IE. Frequently, eastern storms are related to northerly storms, but depending on atmospheric conditions, northerly winds in this region do not always promote eastern storms and vice versa. At present, eastern storms in the NWMed region are responsible of very high wave heights (i.e. significant wave heights of 8 m and maxima of 14 m) and important erosive episodes (Palanques et al., 2006; Sanchez-Vidal et al., 2012). Possibly, during periods of high correlation and a remarkable storminess (like RP, EMA and LIAa) both kind of storms were coupled and could have been enhanced intensity or more frequent occurrence. The confluence of both kinds of storms frequently can provoke maxima transport of suspended sediment towards the deep sea (e.g.: Rumín-Caparrós et al., 2013). However, during moments with no correlation, these two types of storms could have been rather decoupled, observing stronger storms in the GoL during the periods of minimum DWF such as the LIAb (Fig. 6a).

The relationship between GoL-DWF and LIW is explored in base to the records of benthic foraminifera diversity index in SL 112 core from the Liguriam Sea (892 m water depth, Schmiedl et al., 2010) (Fig. 6b). An almost opposite behaviour between the two records can be identified for the periods before and after the EMA (Fig. 6b). During the TP and RP maximum ventilation in LIW coexisted with strong GoL-DWF ($r = 0.6$, p value = 0), supporting a contribution of the LIW salt content promoting deep convection in the GoL during these periods. During the EMA low oxygenation values in the LIW may indicate reduced contribution of this water mass to the NWMed that probably led to the recorded progressive slowdown of GoL-DWF. In a general way, it should be noted that during the last 1.5 kyr, both basins records show a rather opposite trend (Fig. 5b) suggesting a decoupling between the two water masses ($r = -0.5$, p value = 0). Interestingly, an east-west Mediterranean climate sea-saw pattern has been previously described for the last 1.1 kyr (Roberts et al., 2012). Thus, the opposite trends described in the hydro-climatic conditions between Iberia and Turkey during the MCA and LIA could also induce opposite response in the convection cells of the WMDW and the LIW. This Mediterranean bipolar see-saw has been associated with the combination of different climate modes proposing a complex non stationary behaviour of the NAO with other atmospheric modes (Josey et al., 2011; Roberts et al., 2012).

The relationship between DWF in the GoL and the North Atlantic Ocean has previously been established for the last glacial period, at millennial scale, when an opposite correlation was described between the two thermohaline overturning cells. A weakening of North Atlantic DWF occurred during cold stadial phases, associated with surface freshening driven by ice melting events, while GoL-DWF was enhanced, associated with enhanced Mediterranean dry conditions and Northwesterlies intensity over the GoL (Cacho et al., 2000, 2006; Sierro et al., 2005). The comparison of our results to the SS mean size record from the Labrador Sea as a proxy of DWF in this region (Thornalley et al., 2018), also shows a relative opposite trend for the last 1.5 kyr (Fig. 5c). In particular, at sub-centennial scale, this relation is significant during the MCA ($r = -0.5$, p value ≤ 0.0248). The DWF reduction in the Labrador Sea during IE has been associated with surface water freshening, but the forcing mechanism for the previous 1.5 kyr changes remain unclear (Thornalley et al., 2018). Studies focussed on the last decades observations have directly connected Labrador Sea water properties to NAO conditions, through an enhanced westerlies cooling associated with NAO + (i.e: Kieke and Yashayaev, 2015; Ortega et al., 2017). Nevertheless, other factors such as the precise location of the pressure cells can complicate this relation (Kim et al., 2016).

Thus, we explore the potential role of NAO conditions on GoL-DWF for the last 2.5 kyr by comparing our record with the NAO reconstruction from Faust et al. (2016). This comparison suggests again different behaviour during the intervals before and after the EMA (Fig. 5d). During the TP and RP, positive NAO phases are mainly related to GoL-DWF increments, while negative NAO phases are related to rather weak DWF events ($r = 0.3$, p value ≤ 0.0271). For the last 1.5 kyr, although a tempting opposite trend can be observed, no-significant correlation has been obtained, and thus a decrease or increase in DWF occurred indistinctly during both positive and negative NAO phases. For instance, intense negative NAO values during the LIAa coincide with DWF increases, a relation previously suggested for Holocene millennial-centennial time-scale events (Ausín et al., 2015). But, in contrast, during the LIAb weaker negative NAO phases occurred during DWF decreases. These results suggest that GoL-DWF and the NAO do not present a stationary relationship and other mechanisms should interact in the transference of the atmospheric signal from high to medium latitudes. During recent positive NAO phases, a reinforced atmospheric high-pressure system over the western Mediterranean Sea enhances westerly winds circulation, enhancing the E-P balance of the region (Tsimplis and Josey, 2001). However, at annual and multidecadal scales the strength and location of the NAO dipole can be also modulated by the EA and the SCAN patterns (Comas-Bru and McDermott, 2014). Moreover, negative states of the EA pattern can favour the influence of cold and dry winds over the Mediterranean Sea, modulating the air-sea heat exchange (Josey et al., 2011).

In this way, the DWF changes observed in the NWMed region cannot be explained by a single factor such as storm intensity in the GoL, changes in LIW formation or NAO phases and intensity. One of the most remarkable and consistent observation is the rather opposite relationship prior and post the EMA between our GoL-DWF record and both LIW and NAO reconstructions. The EMA climate conditions have been described by several studies as cold and unstable in the northern hemisphere and especially in Europe (Helama et al., 2017 and references therein). Consequently, we propose that these changes during the EMA responded to a variation in the interplay of different atmospheric modes. Such a change has also been described by Sánchez-López et al. (2016) over the Iberian Peninsula, who proposed the dominance of opposite/similar signs in the NAO/EA phases before/after the EMA. Interestingly, changes in the EA/WR and NAO patterns produce opposite hydrological responses in the western-eastern basins of the Mediterranean Sea (Josey et al., 2011). Such a situation could explain the

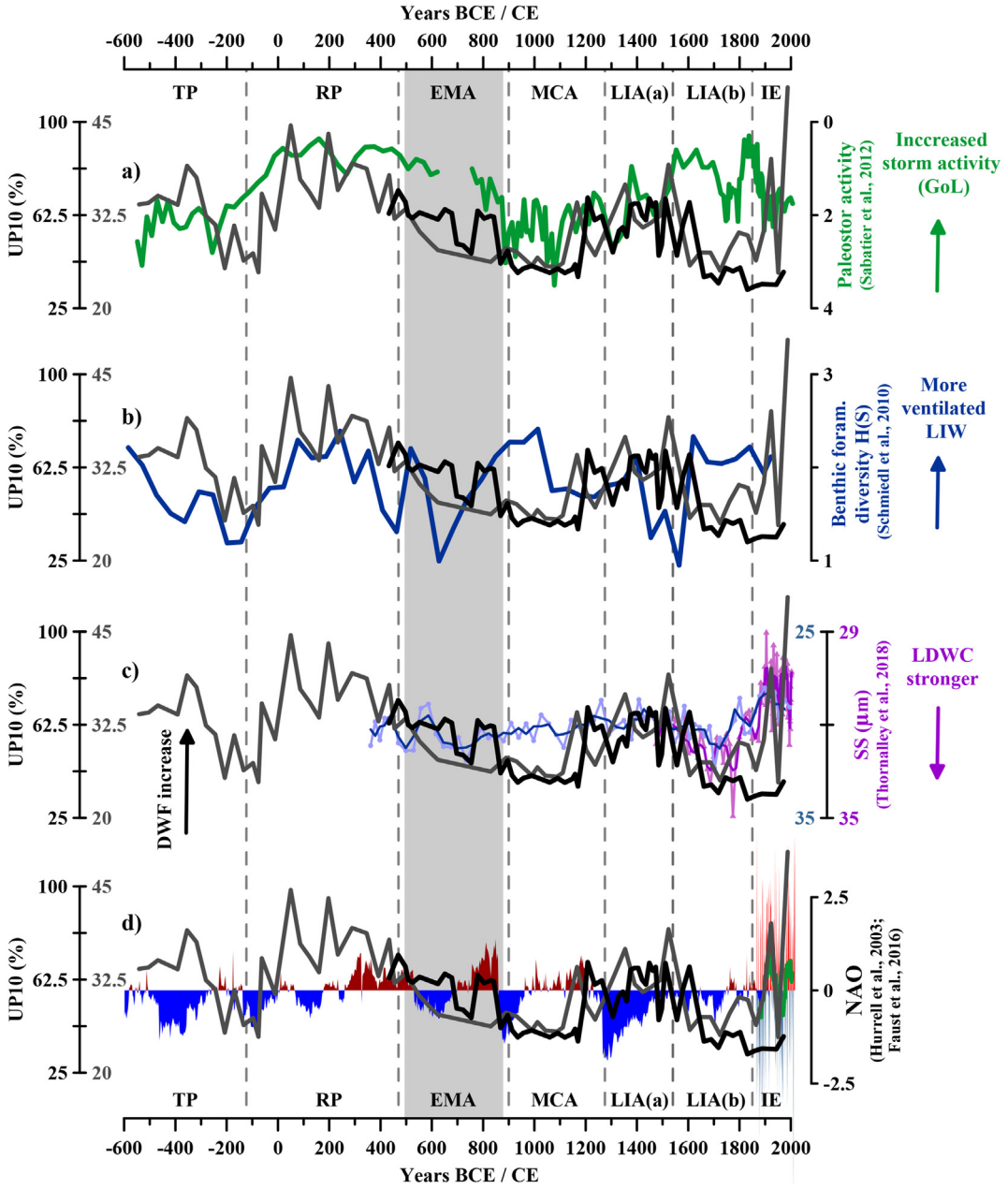

Fig. 6. UP10 record from NMin2 core (de-carbonated fraction) and from NMin1 core (total fraction) are represented in black and grey, respectively, using left axes and compared to: a) Paleostorm activity (Sabatier et al., 2012) in the Gulf of Lion (GoL); b) Benthic foraminifera diversity in the eastern Mediterranean Sea (Schmiedl et al., 2010); LIW: Levantine Intermediate Water. c) Labrador Deep-Water Current (LDWC) reconstructed by Sortable silt (SS) mean grain-size (Thornalley et al., 2018); d) North Atlantic Oscillation (NAO) for the instrumental period (green plot: running averaged 20 yr; Hurrell et al., 2003) and reconstruction for the last 2.5 kyr (Faust et al., 2016). (For interpretation of the references to colour in this figure legend, the reader is referred to the web version of this article.)

described Mediterranean see-saw in both hydrological conditions (Roberts et al., 2012) and GoL-DWF and LIW intensity after the EMA (Fig. 5b). This would support an enhancement in the influence of the EA/WR patterns over the Mediterranean after the EMA (Roberts et al., 2012). A negative state of EA/WR pattern would enhance GoL-DWF and reduce LIW formation and vice versa for a positive pattern (Josey et al., 2011).

5. Conclusions

The evolution of DWF in the Gulf of Lion (GoL) during the last 2.5 kyr is analysed using the grain-size parameter "UP10" (fraction > 10 µm) from two multicores recovered at the sediment drift north of Minorca (NMin). The suitability of the UP10 parameter to track the intensity of deep-water currents related to DWF events has been tested through data from two moorings deployed in the GoL and the NMin regions during 2012–2014. Events of DWF are detected in both moorings by increases in deep-water currents, which reached up to 24 cm s^{-1} in the NMin location, the closest one to the studied sediment cores. Grain-size analyses of settling particles from sediment traps, reveal the appearance of a particular mode (40–100 µm) in samples related to DWF events, a distribution that agrees with those from sediment samples with high UP10 values and interpreted to reflect enhanced deep sea currents.

The sediment core results characterized the Roman Period (RP; 123 BCE-470 CE) like a period of intense DWF. After that, during the Early Middle Ages (EMA; 470–900 CE) intense DWF also occurred but a progressive decrease has been observed until the Medieval Climate

Anomaly (MCA; 900–1275 CE), which is mostly characterized by relatively weak overturning conditions with the exception of the ending century. Our data depict the Little Ice Age (LIA; 1275–1850 CE) in two substages: i) The LIAa with enhanced overturning that started by the end of the MCA ii) LIAb with reduced GoL overturning. Thus, strongest DWF rates took place during rather warm periods, as RP as well as the LIAa, and according to the SST records from the NMin region. When the UP10 is compared to the SST evolution from the GoL, intense DWF occurred during both cold and relatively warm periods.

Therefore, these observations point out that SST was not the only critical factor determining the DWF during the last 2.5 kyr and thus, buoyancy loss was not only driven by SST cooling. Based on our NMin-SST data, we propose that warmer springs played an important role in DWF by increasing the Evaporation-Precipitation balance and favouring buoyancy loss by increased salinity. Such a connection between GoL-DWF and regional hydrological conditions is further supported by coherent covariation between our record and a humidity record from the Iberian Peninsula during the last 1.5 kyr. However, exploring sea surface salinity changes during the past by means of independent proxies to SST reconstructions would likely provide clues in the control of deep water overturning at millennial and centennial, or even, decadal time scales.

The comparison of our GoL-DWF record with other oceanographic-climatic records highlights a complex interaction of different regional atmospheric and oceanic factors to explain the DWF evolution of the last 2.5 kyr. Overall, we describe a major change in the behaviour of the GoL-DWF during the EMA. Previously to the EMA, strong GoL-DWF occurred coincident to strong LIW ventilation and positive NAO phases. In contrast, after the EMA GoL-DWF and LIW present opposite trends and any clear relation is evident with the NAO index. This post-EMA situation is consistent with a previous described east-west climate seasaw in the Mediterranean region and could respond to a stronger influence of the EA/WR pattern that would complicate the NAO influence over the region.

Supplementary data to this article can be found online at https://doi.org/10.1016/j.gloplacha.2019.03.012.

Acknowledgments

We thank the anonymous reviewers for their very useful comments and discussions on this work. ERC-Consolidator Grant TIMED (683237), CHIMERA (CTM2016-75411-R), Consolider-Redes (CTM2014-59111-REDC) and PERSEUS (FP7-OCEAN-2011-3-287600) financially supported this research. We thank Generalitat de Catalunya Grups de Recerca Consolidats for grant 2017 SGR 315 to GRC Geociències Marines. MINMC06 cores were recovered during the HERMES 3 cruise in 2006 on board R/V Thethys II. We are in debt with the crew and scientists onboard SOCIB and Lluerna for their help in the mooring deployment and recovery.

We are grateful to M. Guart (Dept. de Dinàmica de la Terra i de l'Oceà, Universitat de Barcelona) for her help in the laboratory. Mercè Cisneros benefited from a fellowship of the University of Barcelona. Isabel Cacho thanks the ICREA-Academia programme from the Generalitat de Catalunya.

Data availability

Datasets related to this article can be found at https://data.mendeley.com/datasets/mymcnbhkpm/draft?a=1182c022-4439-46ed-8404-322e6262eb02, an open-source online data repository hosted at Mendeley Data.

References

Agrawal, Y.C., McCave, I.N., Riley, J.B., 1991. Laser diffraction size analysis. In: Syvitski, J.P.M. (Ed.), Principles, Methods, and Application of Particle Size Analysis. Cambridge University Press, Cambridge, pp. 119–129.

Ausín, B., Flores, J.A., Sierro, F.J., Cacho, I., Hernández-Almeida, I., Martrat, B., Grimalt, J.O., 2015. Atmospheric patterns driving Holocene productivity in the Alboran Sea (Western Mediterranean): a multiproxy approach. Holocene 25, 1–13. https://doi.org/10.1177/0959683614565952.

Barnston, A.G., Livezey, R.E., 1987. Classification, seasonality and persistence of low-frequency atmospheric circulation patterns. Mon. Weather Rev. 115, 1083–1126. https://doi.org/10.1175/1520-0493(1987) 115<1083:CSAPOL>2.0.CO;2.

Bethoux, J., Gentili, B., Morin, P., Nicolas, E., Pierre, C., Ruiz-Pino, D., 1999. The Mediterranean Sea: a miniature ocean for climatic and environmental studies and a key for the climatic functioning of the North Atlantic. Prog. Oceanogr. 44, 131–146. https://doi.org/10.1016/S0079-6611(99)00023-3.

Bethoux, J.P., Durrieu de Madron, X., Nyffeler, F., Tailliez, D., 2002. Deep water in the western Mediterranean: Peculiar 1999 and 2000 characteristics, shelf formation hypothesis, variability since 1970 and geochemical inferences. J. Mar. Syst. 33–34, 117–131. https://doi.org/10.1016/S0924-7963(02)00055-6.

Beuvier, J., Sevault, F., Herrmann, M., Kontoyiannis, H., Ludwig, W., Rixen, M., Stanev, E., Béranger, K., Somot, S., 2010. Modeling the Mediterranean Sea interannual variability during 1961–2000: Focus on the Eastern Mediterranean Transient. J. Geophys. Res. 115, C08017. https://doi.org/10.1029/2009JC005950.

Bosse, A., Testor, P., Houpert, L., Damien, P., Prieur, L., Hayes, D., Taillandier, V., Durrieu de Madron, X., d'Ortenzio, F., Coppola, L., Karstensen, J., Mortier, L., 2016. Scales and dynamics of Submesoscale Coherent Vortices formed by deep convection in the northwestern Mediterranean Sea: Vortices in the NW Mediterranean Sea. J. Geophys. Res. 121, 7716–7742. https://doi.org/10.1002/2016JC012144.

Bosse, A., Testor, P., Mayot, N., Prieur, L., D'Ortenzio, F., Mortier, L., Le Goff, H., Gourcuff, C., Coppola, L., Lavigne, H., Raimbault, P., 2017. A submesoscale coherent vortex in the Ligurian Sea: from dynamical barriers to biological implications. J. Geophys. Res. https://doi.org/10.1002/2016JC012634.

Bryden, H.L., Stommel, H.M., 1984. Limiting processes that determine basic features of the circulation in the Mediterranean Sea. Oceanol. Acta 7 (3), 289–296.

Bueh, C., Nakamura, H., 2007. Scandinavian pattern and its climatic impact. Q. J. R. Meteorol. Soc. 133, 2117–2131. https://doi.org/10.1002/qj.173.

Cacho, I., Grimalt, J.O., Pelejero, C., Canals, M., Sierro, F.J., Flores, J.A., Shackleton, N.J., 1999. Dansgaard-Oeschger and Heinrich event imprints in Alboran Sea temperatures. Paleoceanography 14, 698–705.

Cacho, I., Grimalt, J.O., Sierro, F.J., Shackleton, N., Canals, M., 2000. Evidence for enhanced Mediterranean thermohaline circulation during rapid climatic coolings. Earth Planet. Sci. Lett. 183, 417–429.

Cacho, I., Shackleton, N., Elderfield, H., Sierro, F.J., Grimalt, J.O., 2006. Glacial rapid variability in deep-water temperature and $\delta^{18}O$ from the Western Mediterranean Sea. Quat. Sci. Rev. 25, 3294–3311. https://doi.org/10.1016/j.quascirev.2006.10.004.

Canals, M., Puig, P., de Madron, X.D., Heussner, S., Palanques, A., Fabres, J., 2006. Flushing submarine canyons. Nature 444, 354–357. https://doi.org/10.1038/nature05271.

Cassou, C., Minvielle, M., Terray, L., Périgaud, C., 2010. A statistical dynamical scheme for reconstructing ocean forcing in the Atlantic. Part I: weather regimes as predictors for ocean surface variable. Clim. Dyn. 36 (1–2), 19–39.

Cisneros, M., Cacho, I., Frigola, J., Canals, M., Masqué, P., Martrat, B., Casado, M., Grimalt, J.O., Pena, L.D., Margaritelli, G., Lirer, F., 2016. Sea surface temperature variability in the central-western Mediterranean Sea during the last 2700 years: a multi-proxy and multi-record approach. Clim. Past 12, 849–869. https://doi.org/10.5194/cp-12-849-2016.

Comas-Bru, L., McDermott, F., 2014. Impacts of the EA and SCA patterns on the European twentieth century NAO-winter climate relationship: Impacts of EA and SCA patterns on NAO-winter climate relationship. Q. J. R. Meteorol. Soc. 140, 354–363. https://doi.org/10.1002/qj.2158.

Deser, C., Alexander, M.A., Xie, S.P., Phillips, A.S., 2010. Sea surface temperature variability: patterns and Mechanisms. Annu. Rev. Mar. Sci. 2, 115–143. https://doi.org/10.1146/annurev-marine-120408-151453.

Durrieu de Madron, X., Houpert, L., Puig, P., Sanchez-Vidal, A., Testor, P., Bosse, A., Estournel, C., Somot, S., Bourrin, F., Bouin, M.N., Beauverger, M., Beguery, L., Calafat, A., Canals, M., Cassou, C., Coppola, L., Dausse, D., D'Ortenzio, F., Font, J., Heussner, S., Kunesch, S., Lefevre, D., Le Goff, H., Martín, J., Mortier, L., Palanques, A., Raimbault, P., 2013. Interaction of dense shelf water cascading and open-sea convection in the northwestern Mediterranean during winter 2012: Shelf Cascading and open-sea convection. Geophys. Res. Lett. 40, 1379–1385. https://doi.org/10.1002/grl.50331.

Durrieu de Madron, X., Ramondenc, S., Berline, L., Houpert, L., Bosse, A., Martini, S., Guidi, L., Conan, P., Curtil, C., Delsaut, N., Kunesch, S., Ghiglione, J.F., Marsaleix, P., Pujo-Pay, M., Séverin, T., Testor, P., Tamburini, C., the ANTARES collaboration, 2017. Deep sediment resuspension and thick nepheloid layer generation by open-ocean convection: BNL generation by open-oean convection. J. Geophys. Res. 122, 2291–2318. https://doi.org/10.1002/2016JC012062.

Estournel, C., Testor, P., Damien, P., D'Ortenzio, F., Marsaleix, P., Conan, P., Kessouri, F., Durrieu de Madron, X., Coppola, L., Lellouche, J.-M., Belamari, S., Mortier, L., Ulses, C., Bouin, M.-N., Prieur, L., 2016. High resolution modeling of dense water formation in the north-western Mediterranean during winter 2012-2013: processes and budget: Modeling of dense water convection. J. Geophys. Res. 121, 5367–5392. https://doi.org/10.1002/2016JC011935.

Faust, J.C., Fabian, K., Milzer, G., Giraudeau, J., Knies, J., 2016. Norwegian fjord sediments reveal NAO related winter temperature and precipitation changes of the past 2800 years. Earth Planet. Sci. Lett. 435, 84–93. https://doi.org/10.1016/j.epsl.2015.12.003.

Frigola, J., Moreno, A., Cacho, I., Canals, M., Sierro, F.J., Flores, J.A., Grimalt, J.O., Hodell, D.A., Curtis, J.H., 2007. Holocene climate variability in the western

Mediterranean region from a deepwater sediment record. Paleoceanography 22. https://doi.org/10.1029/2006PA001307.
Frigola, J., Moreno, A., Cacho, I., Canals, M., Sierro, F.J., Flores, J.A., Grimalt, J.O., 2008. Evidence of abrupt changes in Western Mediterranean Deep Water circulation during the last 50kyr: a high-resolution marine record from the Balearic Sea. Quat. Int. 181, 88–104. https://doi.org/10.1016/j.quaint.2007.06.016.
Gambacort, G., Bersezio, R., Erba, E., 2014. Sedimentation in the Tethyan pelagic realm during the Cenomaniam: monotonous settling or active redistribution? Palaeogeogr. Palaeoclimatol. Palaeoecol. 409, 301–319.
Hall, I.R., McCave, I.N., 2000. Palaeocurrent reconstruction, sediment and thorium focussing on the Iberian margin over the last 140 ka. Earth Planet. Sci. Lett. 178, 151–164.
Helama, S., Jones, P.D., Briffa, K.R., 2017. Dark Ages Cold Period: a literature review and directions for future research. The Holocene 1–7. https://doi.org/10.1177/0959683617693898.
Houpert, L., Durrieu de Madron, X., Testor, P., Bosse, A., D'Ortenzio, F., Bouin, M.N., Dausse, D., Le Goff, H., Kunesch, S., Labaste, M., Coppola, L., Mortier, L., Raimbault, P., 2016. Observations of open-ocean deep convection in the northwestern Mediterranean Sea: Seasonal and interannual variability of mixing and deep water masses for the 2007-2013 Period: DEEP CONVECTION OBS. NWMED 2007-2013. J. Geophys. Res. 121, 8139–8171. https://doi.org/10.1002/2016JC011857.
Hüneke, H., Stow, D.A.V., 2008. Identification of ancient contourites: Problems and palaeoceanographic significance. In: Rebesco, M., Camerlenghi, A. (Eds.), Contourites, Developments in Sedimentology 60. Elsevier, Amsterdam, pp. 323–344.
Hurrell, J.W., 1995. Decadal Trends in the North Atlantic Oscillation: regional temperatures and precipitation. Science 269, 676–679. https://doi.org/10.1126/science.269.5224.676.
Hurrell, J.W., Kushnir, Y., Ottersen, G., Visbeck, M., 2003. The North Atlantic oscillation: climate significance and environmental impact. Geophys. Monogr. Ser. 134. https://doi.org/10.1029/134GM01.
Incarbona, A., Martrat, B., Mortyn, P.G., Sprovieri, M., Ziveri, P., Gogou, A., Jordà, G., Xoplaki, E., Luterbacher, J., Langone, L., Marino, G., Rodríguez-Sanz, L., Triantaphyllou, M., Di Stefano, E., Grimalt, J.O., Tranchida, G., Sprovieri, R., Mazzola, S., 2016. Mediterranean circulation perturbations over the last five centuries: relevance to past Eastern Mediterranean Transient-type events. Sci. Rep. 6. https://doi.org/10.1038/srep29623.
Josey, S.A., 2003. Changes in the heat and freshwater forcing of the Eastern Mediterranean and their influence on DeepWater Formation. J. Geophys. Res. 108, 3237. https://doi.org/10.1029/2003JC001778.
Josey, S.A., Somot, S., Tsimplis, M., 2011. Impacts of atmospheric modes of variability on Mediterranean Sea surface heat exchange. J. Geophys. Res. 116. https://doi.org/10.1029/2010JC006685.
Kieke, D., Yashayaev, I., 2015. Studies of Labrador Sea Water formation and variability in the subpolar North Atlantic in the light of international partnership and collaboration. Progr. Iceanogr. 132, 220–232. https://doi.org/10.1016/j.pocean.2014.12.010.
Kim, W.M., Yeager, S., Chang, P., Danabasoglu, G., 2016. Atmospheric Conditions Associated with Labrador Sea Deep Convection: New Insights from a Case Study of the 2006/07 and 2007/08 Winters. Am. Meteorol. Soc. 29, 5281–5297. https://doi.org/10.1175/JCLI-D-15-0527.1.
Konert, M., Vandenberghe, J., 1997. Comparison of laser grain-size analysis with pipette and sieve analysis: a solution for the underestimation of the clay fraction. Sedimentology 44, 523–535.
Krichak, S.O., Alpert, P., 2005. Decadal trends in the east Atlantic west Russia pattern and Mediterranean precipitation. Int. J. Climatol. 25, 183–192. https://doi.org/10.1002/joc.1124.
Li, M.Z., Amos, C.L., 2001. SEDTRANS96: the upgraded and better calibrated sediment-transport model for continental shelves. Comput. Geosci. 27, 619–645.
Lionello, P., Malanott-Rizzoli, R., Boscolo, R., Alpert, P., Artale, V., Li, L., Luterbacher, J., May, W., Trigo, R., Tsimplis, M., Ulbrich, U., Xoplaki, E., 2006. The Mediterranean climate: an overview of the main characteristics and issues. In: Mediterranean Climate Variability (MedClivar). Elsevier, Amsterdam, pp. 1–26.
López-Jurado, J.L., González-Pola, C., Vélez-Belchi, P., 2005. Observation of an abrupt disruption of the long-term warming trend at the Balearic Sea, western Mediterranean Sea, in summer 2005. Geophys. Res. Lett. 32, 1–4. https://doi.org/10.1029/2005GL024430.
Margalef, R., 1985. In: Margalef, R. (Ed.), Introduction to the Mediterranean. A Western Mediteranean. Oxford, Pergamon Press, pp. 1–16.
Margaritelli, G., Cisneros, M., Cacho, I., Vallefuoco, M., Rettori, R., Lirer, F., 2018. Climatic variability over the last 3000 years in the central-western Mediterranean Sea (Menorca Basin) detected by planktonic foraminifera and stable isotope records. Glob. Planet. Changes 169, 179–187. https://doi.org/10.1016/j.gloplacha.2018.07.012.
Margirier, F., Testor, P., Bosse, A., L'Hévéder, L., Mortier, L., Smeed, D., 2017. Characterization of Convective Plumes associated with Oceanic deep convection in the Northwestern Mediterranean from high-resolution in situ data collected by gliders. J. Geophys. Res. 122, 1–13. https://doi.org/10.1002/2016JC012633.
Martín, J., Miquel, J.C., Khripounoff, A., 2010. Impact of open sea deep convection on sediment remobilization in the western Mediterranean. Geophys. Res. Lett. 37, L13604. https://doi.org/10.1029/2010GL043704.
McCave, I.N., Bryant, R.J., Cook, H.F., Coughanowr, C.A., 1986. Evaluation of a laser-diffraction-size analyzer for use with natural sediments. J. Sediment. Res. 56, 561–564.
McCave, I.N., Manighetti, B., Robinson, S.G., 1995. Sortable silt and fine sediment size/composition slicing: parameters for paleocurrent speed and paleoceanography. Paleoceanography 10, 593–610.
McCave, I.N., Thornalley, D.J.R., Hall, I.R., 2017. Relation of sortable silt grain-size to deep-sea current speeds: Calibration of the 'Mud Current Meter'. Deep-Sea Res. Part I Oceanogr. Res. Pap. https://doi.org/10.1016/j.dsr.2017.07.003.
MEDOC Group, 1970. Observation of formation of Deep Water in the Mediterranean Sea. Nature 227, 1037–1040.
Millot, C., 1999. Circulation in the Western Mediterranean Sea. J. Mar. Syst. 20, 423–442.
Morellón, M., Valero-Garcés, B., Vegas-Vilarrúbia, T., González-Sampériz, P., Romero, Ó., Delgado-Huertas, A., Mata, P., Moreno, A., Rico, M., Corella, J.P., 2009. Lateglacial and Holocene palaeohydrology in the western Mediterranean region: the Lake Estanya record (NE Spain). Quat. Sci. Rev. 28, 2582–2599. https://doi.org/10.1016/j.quascirev.2009.05.014.
Morellón, M., Valero-Garcés, B., González-Sampériz, P., Vegas-Vilarrúbia, T., Rubio, E., Rieradevall, M., Delgado-Huertas, A., Mata, P., Romero, Ó., Moreno, A., Engstrom, D.R., López-Vicente, M., Navas, A., Soto, J., 2011. Climate changes and human activities recorded in the sediments of Lake Estanya (NE Spain) during the Medieval Warm Period and Little Ice Age. J. Paleolimnol. 46, 423–452. https://doi.org/10.1007/s10933-009-9346-3.
Moreno, A., Pérez, A., Frigola, J., Nieto-Moreno, V., Rodrigo-Gámiz, M., Martrat, B., González-Sampériz, P., Morellón, M., Martín-Puertas, C., Corella, J.P., Belmonte, A., Sancho, C., Cacho, I., Herrera, G., Canals, M., Grimalt, J.O., Jiménez-Espejo, F., Martínez-Ruiz, F., Vegas-Vilarrúbia, T., Valero-Garcés, B.L., 2012. The Medieval Climate Anomaly in the Iberian Peninsula reconstructed from marine and lake records. Quat. Sci. Rev. 43, 16–32. https://doi.org/10.1016/j.quascirev.2012.04.007.
Ortega, P., Robson, J., Sutton, R.T., Andrews, M.B., 2017. Mechanisms of decadal variability in the Labrador Sea and the wider North Atlantic in a high-resolution climate model. Clim. Dyn. 49, 2625–2647. https://doi.org/10.1007/s00382-016-3467-y.
Palanques, A., Durrieu de Madron, X., Puig, P., Fabres, J., Guillén, J., Calafat, A., Canals, M., Heussner, S., Bonnin, J., 2006. Suspended sediment fluxes and transport processes in the Gulf of Lions submarine canyons, the role of storms and dense water cascading. Mar. Geol. 234, 43–61. https://doi.org/10.1016/j.margeo.2006.09.002.
Pattiaratchi, C., Hollings, B., Woo, M., Welhena, T., 2011. Dense shelf water formation along the south-west Australian inner shelf. Geophys. Res. Lett. 38, L10609. https://doi.org/10.1029/2011GL046816.
Puig, P., Palanques, A., Orange, D.L., Lastras, G., Canals, M., 2008. Dense shelf water cascades and sedimentary furrow formation in the Cap de Creus Canyon, northwestern Mediterranean Sea. Cont. Shelf Res. 28, 2017–2030.
Puig, P., de Madron, X.D., Salat, J., Schroeder, K., Martín, J., Karageorgis, A.P., Palanques, A., Roullier, F., Lopez-Jurado, J.L., Emelianov, M., Moutin, T., Houpert, L., 2013. Thick bottom nepheloid layers in the western Mediterranean generated by deep dense shelf water cascading. Prog. Oceanogr. 111, 1–23. https://doi.org/10.1016/j.pocean.2012.10.003.
Roberts, N., Moreno, A., Valero-Garcés, B.L., Corella, J.P., Jones, M., Allcock, S., Woodbridge, J., Morellón, M., Luterbacher, J., Xoplaki, E., Türkeş, M., 2012. Palaeolimnological evidence for an east–west climate see-saw in the Mediterranean since AD 900. Glob. Planet. Chang. 84–85, 23–34. https://doi.org/10.1016/j.gloplacha.2011.11.002.
Rodrigo-Gámiz, M., Martínez-Ruiz, F., Jiménez-Espejo, F.J., Gallego-Torres, D., Nieto-Moreno, V., Romero, O., Ariztegui, D., 2011. Impact of climate variability in the western Mediterranean during the last 20,000 years: oceanic and atmospheric responses. Quat. Sci. Rev. 30, 2018–2034. https://doi.org/10.1016/j.quascirev.2011.05.011.
Rohling, E.J., Marino, G., Grant, K.M., 2015. Mediterranean climate and oceanography, and the periodic development of anoxic events (sapropels). Earth Sci. Rev. 143, 62–97. https://doi.org/10.1016/j.earscirev.2015.01.008.
Roveri, M., Manzi, V., Bergamasco, A., Falcieri, F.M., Gennari, R., Lugli, S., Schreiber, B.C., 2014. Dense shelf water cascading and Messinian canyons: a new scenario for the Mediterranean salinity crisis. Am. J. Sci. 314, 751–784.
Rumín-Caparrós, A., Sanchez-Vidal, A., Calafat, A., Canals, M., Martín, J., Puig, P., Pedrosa-Pamies, R., 2013. External forcings, oceanographic processes and particle flux dynamics in Cap de Creus submarine canyon, NW Mediterranean Sea. Biogeosciences 10, 3493–3505. https://doi.org/10.5194/bg-10-3493-2013.
Sabatier, P., Dezileau, L., Colin, C., Briqueu, L., Bouchette, F., Martinez, P., Siani, G., Raynal, O., Von Grafenstein, U., 2012. 7000 years of paleostorm activity in the NW Mediterranean Sea in response to Holocene climate events. Quat. Res. 77, 1–11. https://doi.org/10.1016/j.yqres.2011.09.002.
Sánchez-López, G., Hernández, A., Pla-Rabes, S., Trigo, R.M., Toro, M., Granados, I., Sáez, A., Masqué, P., Pueyo, J.J., Rubio-Inglés, M.J., Giralt, S., 2016. Climate reconstruction for the last two millennia in central Iberia: the role of East Atlantic (EA), North Atlantic Oscillation (NAO) and their interplay over the Iberian Peninsula. Quat. Sci. Rev. 149, 135–150. https://doi.org/10.1016/j.quascirev.2016.07.021.
Sanchez-Vidal, A., Pascual, C., Kerherveé, P.A., Calafat, A., Heussner, S., Palanques, A., Durrieu de Madron, X., Canals, M., Puig, P., 2008. Impact of dense shelf water cascading on the transfer of organic matter to the deep Western Mediterranean Basin. Geo. Phys. Res. Lett. 35, L05605. https://doi.org/10.1029/2007GL032825.
Sanchez-Vidal, A., Canals, M., Calafat, A., Lastras, G., Pedrosa-Pàmies, R., Menéndez, M., Medina, R., Company, J.B., Hereu, B., Romero, J., Alcoverro, T., 2012. Impacts on the deep-sea ecosystem by a severe coastal storm. PLoS One 7, e30395. https://doi.org/10.1371/journal.pone.0030395.
Sanchez-Vidal, A., Llorca, M., Farré, M., Canals, M., Barceló, D., Puig, P., Calafat, A., 2015. Delivery of unprecedented amounts of perfluoroalkyl substances towards the deep-sea. Sci. Total Environ. 526, 41–48. https://doi.org/10.1016/j.scitotenv.2015.04.080.
Schmiedl, G., Kuhnt, T., Ehrmann, W., Emeis, K.-C., Hamann, Y., Kotthoff, U., Dulski, P., Pross, J., 2010. Climatic forcing of eastern Mediterranean deep-water formation and benthic ecosystems during the past 22 000 years. Quat. Sci. Rev. 29, 3006–3020. https://doi.org/10.1016/j.quascirev.2010.07.002.

Schroeder, K., Josey, S.A., Herrmann, M., Grignon, L., Gasparini, G.P., Bryden, H.L., 2010. Abrupt warming and salting of the Western Mediterranean Deep Water after 2005: Atmospheric forcings and lateral advection. J. Geophys. Res. 115. https://doi.org/10.1029/2009JC005749.

Schroeder, K., Haza, A.C., Griffa, A., Özgökmen, T.M., Poulain, P., Gerin, R., Peggion, G., Rixen, M., 2011. Relative dispersion in the liguro-provencal basin: from sub-mesoscale to mesoscale. Deep-Sea Res. I 58, 861–882.

Sicre, M.-A., Jalali, B., Martrat, B., Schmidt, S., Bassetti, M.-A., Kallel, N., 2016. Sea surface temperature variability in the North Western Mediterranean Sea (Gulf of Lion) during the Common Era. Earth Planet. Sci. Lett. 456, 124–133. https://doi.org/10.1016/j.epsl.2016.09.032.

Sierro, F.J., Hodell, D.A., Curtis, J.H., Flores, J.A., Reguera, I., Colmenero-Hidalgo, E., Bárcena, M.A., Grimalt, J.O., Cacho, I., Frigola, J., Canals, M., 2005. Impact of iceberg melting on Mediterranean thermohaline circulation during Heinrich events: impact of Iceberg melting in the Mediterranean. Paleoceanography 20, PA2019. https://doi.org/10.1029/2004PA001051.

Somavilla, R., González-Pola, C., Rodriguez, C., Josey, S.A., Sánchez, R.F., Lavín, A., 2009. Large changes in the hydrographic structure of the Bay of Biscay after the extreme mixing of winter 2005. J. Geophys. Res. 114, C01001. https://doi.org/10.1029/2008JC004974.

Somot, S., Sevault, F., Déqué, M., 2006. Transient climate change scenario simulation of the Mediterranean Sea for the twenty-first century using a high-resolution ocean circulation model. Clim. Dyn. 27, 851–879.

Somot, S., Houpert, L., Sevault, F., Testor, P., Bosse, A., Taupier-Letage, I., Bouin, M.-N., Waldman, R., Cassou, C., Sanchez-Gomez, E., Durrieu de Madron, X., Adloff, F., Nabat, P., Herrmann, M., 2016. Characterizing, modelling and understanding the climate variability of the deep water formation in the North-Western Mediterranean Sea. Clim. Dyn. https://doi.org/10.1007/s00382-016-3295-0.

Stabholz, M., Durrieu de Madron, X., Canals, M., Khripounoff, A., Taupier-Letage, I., Testor, P., Heussner, S., Kerhervé, P., Delsaut, N., Houpert, L., Lastras, G., Dennielou, B., 2013. Impact of open-ocean convection on particle fluxes and sediment dynamics in the deep margin of the Gulf of Lions. Biogeosciences 10, 1097–1116. https://doi.org/10.5194/bg-10-1097-2013.

Stanley, D.J. (Ed.), 1972. The Mediterranean Sea: A Natural Sedimentation Laboratory. 765 Dowden, Hutchinson & Ross, Stroudsbourg, PA.

Stommel, H., 1972. Deep winter-time convection in the Western Mediterranean Sea. In: Gordon, A.L. (Ed.), Studies in Physical Oceanography, a Tribute to Georg Wiist on his 80th birthday. 2. Gordon & Breach, pp. 207–218.

Stommel, H., Bryden, H., Mangelsd, P., 1973. Does some of Mediterranean outflow come from great depth? Pure Appl. Geophys. 105 (4), 879–889.

Testor, P., Gascard, J.C., 2006. Post-convection spreading phase in the Northwestern Mediterranean Sea. Deep-Sea Res. Part I Oceanogr. Res. Pap. 53, 869–893. https://doi.org/10.1016/j.dsr.2006.02.004.

Thornalley, D.J.R., Oppo, D.W., Ortega, P., Robson, J.I., Brierley, C.M., Davis, R., Hall, I.R., Moffa-Sanchez, P., Rose, N.L., Spooner, P.T., Yashayaev, I., Keigwin, Ll.D., 2018. Anomalously weak Labrador Sea convection and Atlantic overturning during the past 150 years. Nature 556, 227–230. https://doi.org/10.1038/s41586-018-0007-4.

Trigo, R., Xoplaki, E., Zorita, E., Lutherbacher, J., Krichak, S.O., Alpert, P., Jacobeit, J., Sáenz, J., Fernández, J., González-Rouco, F., Garcia-Herrera, R., Rodo, X., Brunetti, M., Nanni, T., Maugeri, M., Tükes, M., Gimeno, L., Ribera, P., Brunet, M., Trigo, I.F., Crepon, M., Mariotti, A., 2006. Relations between variability in the Mediterranean Region and Mid-Latitude Variability. In: Mediterranean Climate Variability (MedClivar). Elsevier, Amsterdam, pp. 178–226.

Tsimplis, M.N., Josey, S.A., 2001. Forcing of the Mediterranean Sea level by atmospheric oscillations over the North Atlantic. Geophys. Res. Lett. 28, 803–806. https://doi.org/10.1029/2000GL012098.

Velasco, J.P.B., Baraza, J., Canals, M., 1996. La depresión periférica y el lomo contourítico de Menorca: evidencias de la actividad de corrientes de fondo al N del Talud Balear. Geogaceta 20, 359–362.

Waldman, R., Somot, S., Herrmann, M., Bosse, A., Caniaux, G., Estournel, C., Houpert, L., Prieur, L., Sevault, F., Testor, P., 2017. Modeling the intense 2012-2013 dense water formation event in the northwestern Mediterranean Sea: evaluation with an ensemble simulation approach. J. Geophys. Res. 122 (2), 1297–1324.

Wallace, J.M., Gutzler, D.S., 1981. Teleconnections in the geopotential height field during the Northern Hemisphere winter. Mon. Weather Rev. 109, 784–812.

Wu, W., Danabasoglu, G., Large, W.G., 2007. On the effects of parameterized Mediterranean Overflow on North Atlantic ocean circulation and climate. Ocean Modell. 19 (1–2), 31–52. https://doi.org/10.1016/j.ocemod.2007.06.003.